Methyl group dynamics in the crystalline alanine dipeptide: A combined computer simulation and inelastic neutron scattering analysis

G. R. Kneller
IBM France, 68-76 Quai de al Rapée, F-75012 Paris, France and Section de Biophysique des Proteines et des Membranes, Departement de Biologie Cellulaire et Moléculaire, C. E. Saclay, 91191 Gif-sur-Yvette, France

W. Doster and M. Settles
Technische Universität München, Physik Dept. E13, D-W8043 Garching, Germany

S. Cusack
E.M.B.L. c/o I.L.L. Avenue des Martyrs, 156X, 38042 Grenoble, France

J. C. Smith
Section de Biophysique des Proteines et des Membranes, Departement de Biologie Cellulaire et Moléculaire, C. E. Saclay, 91191 Gif-sur-Yvette, France

(Received 20 April 1992; accepted 11 September 1992)

The dynamics of the methyl groups in the crystalline alanine dipeptide is examined over a wide range of temperatures using elastic and inelastic neutron scattering experiments and molecular dynamics (MD) simulations of the full crystal. Neutron scattering spectra are calculated from the simulations and directly compared to the experimental profiles. The N-ter and C-ter methyl groups in the molecule have low rotational barriers, i.e., $\lesssim 1$ kcal/mol. They undergo rotations that are activated on time scales faster than ≈ 1 ns at temperatures as low as 50–100 K and are on the picosecond time scale at 150 and 300 K. At 300 K the rotational motion becomes strongly diffusive in the simulation. In contrast, the side-chain methyls possess a significant intramolecular intrinsic torsional barrier, ≈ 3 kcal/mol. As a result, their dynamics consists of librations and rare jumps between wells. The simulations are further analyzed to characterize in detail the motions giving rise to the calculated scattering. Using a quaternion-based method the simulated methyl dynamics is decomposed into rigid-body rotational and translational components. The decomposed motions and their contributions to the calculated neutron profiles are examined.

I. INTRODUCTION

The crystalline state provides structurally well-characterized systems enabling detailed studies of environmental effects on molecular motions. Of particular interest are the effects of nonbonded interactions, such as Coulomb and "soft sphere" interactions, on the dynamics of rotating groups in molecules. The interactions influence the effective potentials of mean force for rotational motion and contribute frictional and collisional dynamical effects. The rotational dynamics of methyl groups in molecular crystals[1–3] serve as examples where nonbonded interactions influence librational oscillations and transitions between equivalent threefold-degenerate conformers.

Methyl group librational and transitional motions typically occur on the picosecond (ps) and nanosecond (ns) time scales at 300 K.[1–3] Motions on these time scales can be probed in detail using the experimental technique of incoherent inelastic neutron scattering spectroscopy and the computational method of classical molecular dynamics simulation. The molecular dynamics method employs empirical potential energy functions. Using the energy functions the equations of motion are integrated over femtosecond time steps so as to build up picosecond time scale trajectories for the atoms in the system. Inelastic neutron scattering[4] involves the measurement of neutron scattering intensities as a function of the energy transfer, ω and momentum transfer, $\mathbf{q}$. In organic molecules incoherent scattering from the hydrogen atoms dominates the measured intensities. Incoherent scattering probes *self-correlations* in motions of atoms. Incoherent scattering can be divided into three types: elastic, quasielastic, and inelastic. The inelastic scattering arises from vibrational motion in the sample. From an analysis of the inelastic scattering the vibrational density of states (frequency distribution) can be extracted. The quasielastic scattering arises from stochastic motions such as conformational transitions or overdamped vibrations. The elastic scattering gives information on the geometry of the motions involved and the associated atomic mean square displacements in the long time limit. The incoherent neutron scattering properties can be directly calculated from the molecular dynamics trajectories to enable a detailed comparison between the experiments and simulations.[5–7]

In this paper we investigate the rotational dynamics of the methyl groups in crystals of the alanine dipeptide, N-methyl-L-alanyl-N-methylamide [CH_3–CONH–$C_\alpha H(C_\beta H_3)$–CONH–CH_3], drawn in Fig. 1. This molecule is one of the simplest model peptide molecules containing the basic fragments necessary for a detailed understanding of the interatomic interactions present in proteins. It has thus been the target of many theoretical studies particularly on the conformational equilibria of the

 0021-9606/92/248864-16$06.00

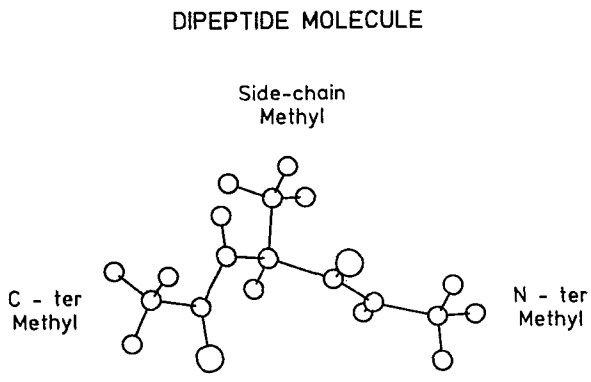

FIG. 1. The alanine dipeptide molecule.

molecule isolated and in water.[8,9]

The dipeptide molecule contains three methyl groups capable of undergoing rotational transitions. Two different contributions to the effective rotational barriers of these methyls can be identified. One is the "intrinsic" potential. This is the dihedral potential that would exist in the absence of environmental effects and is modeled by a specific torsional term in the empirical energy function. The other contribution arises from additional, nonbonded interactions present in the crystal.

In the alanine dipeptide one of the methyl groups is the side chain; the single-bond dihedral is that between the C_α and C_β carbons, these having sp_3 electronic orbitals. The intrinsic (gas phase) rotational barrier for this side chain is expected to be similar to that seen in ethane, i.e., 2.93 kcal/mol,[10] with the minimum in the staggered conformation. The origin of the intrinsic barrier in ethane is mainly overlap (exchange) repulsion between the CH bond orbitals.[11]

Rotational barriers of methyl groups adjacent to double bonds, such as the C-terminal (ψ rotation) and N-terminal (ϕ rotation) methyl groups in the alanine dipeptide, are quite different. In most organic molecules of this type the minimum in the potential energy tends to be in the eclipsed position (not staggered as in ethane). Also, the barriers tend to be much smaller. For example, in acetaldehyde, CH_3CHO the barrier is 1.16 kcal/mol.[12] In acetamide, CH_3CONH_2 an electronic configuration resembling that of the peptide group is adjacent to the C-terminal methyl; the rotational barrier of this molecule is <0.1 kcal/mol.[13] The acetamide rotational potential should strongly resemble that of the C-terminal CH_3 group in the alanine dipeptide (and also the intrinsic contribution to the ψ rotational potential in peptides and proteins). To confirm the above experimental results high-level quantum mechanical calculations were performed on acetaldehyde, acetamide, and N-methylacetamide—the conclusions support strongly the existence of a close-to-zero intrinsic contribution to the dipeptide ϕ and ψ rotational potentials.[14] The above evidence strongly suggests that the methyl groups in the alanine dipeptide come in two sorts; the side chain methyl has an intrinsic barrier of about 3 kcal/mol, whereas the N-ter and C-ter methyls have much smaller intrinsic barriers, close to 0 kcal/mol. In what follows we will loosely refer to these as the "hindered" and "free" methyls. This terminology refers to the intrinsic barrier; in the crystal an effective rotational barrier will exist for all methyls due to the influence of nonbonded interactions.

The unit cell of the crystal contains eight dipeptide molecules arranged in a hydrogen-bonded helical configuration.[15] The local forces between the methyl atoms and atoms from other molecules in the crystal are expected to be dominated by soft-sphere interactions which are modeled by a Lennard-Jones potential in the force field employed in the present simulations. The rotational motion of the methyl groups can be considered in terms of two components—librational oscillations within the rotational potential well and transitions between them. Nonbonded interactions between the methyl group and its environment will play an important role in determining the dynamical characteristics of the rotational transitions and frictional damping effects on the librational modes.

In this paper we use incoherent neutron scattering and molecular dynamics to investigate the 0.1–100 ps time scale dynamics of the hydrogen atoms in the dipeptide molecule. The neutron scattering is dominated by incoherent scattering from the hydrogen atoms. Nine of the 12 hydrogens are in methyl groups, which thus contribute the majority of the scattering intensity. We report neutron scattering measurements made on two spectrometers at the Institut Laue-Langevin in Grenoble, one (IN6) measuring picosecond time scale inelastic and quasielastic spectra and the other (IN13) used to measure elastic scattering originating from motions on time scales faster than ≈ 1 ns.[16] These results are compared with molecular dynamics simulations using the CHARMM program,[17] in which the picosecond time scale motions of the alanine dipeptide are simulated with the crystal environment included using periodic boundary conditions. In the CHARMM force field the intrinsic rotational potential of the alanine side chain is represented by a sinusoidal term with a barrier of 2.86 kcal/mol. The total barrier is thus represented by a sum of this and the contributions due to crystal nonbonded interactions. For the free methyl groups an intrinsic barrier of zero is assigned.

Neutron scattering quantities are directly calculated from the simulations using the time-correlation function formalism.[18,19] For each type of scattering examined a comparison is made between the experimentally derived profile and the simulation equivalent, calculated from all the hydrogens in the molecule. A further analysis is made in which the molecular dynamics trajectories are used to examine different aspects of the methyl group motions. A separation of the various contributions to the simulation neutron spectra is made possible using a method based on Hamilton's quaternion formalism. The method allows the calculation and analysis of the rigid-body methyl group trajectories from the full dynamics results.[20] In this way methyl group rotational and translational contributions to the displacements, transitions, and vibrations are examined. Several dynamical effects seen in the simulations are also clearly present in the experimental samples. However, the simulation-derived and experimental elastic and inelas-

tic spectra are never in quantitative agreement. The possible reasons for the differences are discussed in terms of the incompleteness of the simulation representation of the experimental ensemble of molecules and in terms of the different factors contributing to the experimental data.

The paper is organized as follows. In Sec. II we describe briefly the neutron experimental methods, the MD energy function, and simulation procedure. The quaternion-fit methodology employed for the dynamics trajectory analysis is described together with the methods employed in calculating the neutron scattering properties. In Sec. III the results are given. The experimental and simulation-derived elastic incoherent structure factors (EISFs) are examined as a function of temperature and momentum transfer. The methyl group contributions to the simulation-derived EISFs are analyzed. The time scales and dynamical nature of the rotational methyl group transitions are investigated by analyzing directly the simulated time series of the rotation angle about the C_3 symmetry axis. This angle is identical to the rigid-methyl dihedral angle (X–C–C–H) in the case where the methyl group can be considered a tetrahedron in which the methyl carbon is located at the center and the C_α atom and the hydrogen atoms are at the corners. In the following we will refer to the rotation angle about the C_3 axis also as the "methyl dihedral angle." Finally, the low-frequency ($<300\ \mathrm{cm}^{-1}$) vibrational characteristics are examined using measured inelastic scattering spectra and vibrational frequency distributions and comparing with the corresponding simulation-derived spectra. The concluding discussion is presented in Sec. IV. The combined neutron/simulation approach presents a direct test of the accuracy of present simulation techniques in representing short-range picosecond-time scale condensed phase dynamical effects. Correspondingly, the decomposition of the motions constributing to the simulation-derived scattering reveals a variety of different dynamical effects.

II. METHODS

A. Neutron scattering experiments

The alanine dipeptide was purchased from Bachem Feinchemikalien AG and crystallized from methanol at room temperature[21] yielding a polycrystalline powder for the experiments. Spectra were taken at 150 and 300 K using the IN6 spectrometer with the incident neutron wavelength set at 5.14 Å. The elastic energy resolution was 51 μeV. The spectra were taken in aluminium cells with run times of 3–4 h each. Sample transmissions were about 90%. The raw data were corrected using the programs PRIME and CROSSX at the ILL. These programs normalize the detector responses with respect to an angle-independent standard vanadium sample, normalize each run to the number of incident neutrons, perform slab corrections for the self-shielding and attenuation of singly scattered neutrons, and subtract the cell scattering from the sample+cell scattering. The scattering from the aluminium cells was 1%–3% of the total scattering.

The backscattering spectrometer IN13 with an elastic resolution of 7 μeV was used for high-resolution elastic scattering measurements on the crystals. Elastic scans were performed at temperatures between 22 and 325 K using a liquid-helium cryostat. The q range thus covered was $0.3\ \text{Å}^{-1} < q < 5.5\ \text{Å}^{-1}$. Similar data reduction was performed as for the IN6 experiments, using the programs IQ0 and SQ0 at the ILL. The elastic scan intensities were normalized against the data at the lowest temperature (22 K). The elastic scan experiment was repeated on a different sample and gave the same results.

B. Molecular dynamics simulations

1. Potential energy function

The model used treats all atoms in the system explicitly. The CHARMM energy function employed for the simulations has the following form:

$$V = \sum_{\text{bonds}} k_b(b-b_0)^2 + \sum_{\text{angles}} k_\theta(\theta-\theta_0)^2 + \sum_{\text{dihedrals}} k_\phi(1+\cos[n\phi-\delta]) + \sum_{\text{impropers}} k_\omega(\omega-\omega_0)^2 + \sum_{i,j} 4\epsilon_{ij}\left[\left(\frac{\sigma_{ij}}{r_{ij}}\right)^{12} - \left(\frac{\sigma_{ij}}{r_{ij}}\right)^{6}\right] + \sum_{i,j} \frac{1}{4\pi\epsilon}\frac{q_i q_j}{r_{ij}}. \quad (1)$$

The force field includes *bonded interactions*, comprising bond stretches, bond angle bends, and dihedral angle contributions, and *nonbonded interactions* between pairs (i,j) of atoms. In Eq. (1) b, θ, ϕ, and ω are the bond lengths, angles, dihedrals, and improper torsions at any given configuration and b_0, θ_0, ω_0 are the reference values for these properties; the associated force constants are k_b, k_θ, k_ϕ, and k_ω. For the intrinsic torsions n is the symmetry number of the rotor (e.g., 3 for a methyl group) and δ is the phase angle. The improper dihedral contributions are used to represent out-of-plane deformations of the sp_2 groups. Of particular importance in the present study is the value of the intrinsic torsional term for the methyl groups. For the side-chain methyl this was set as 2.86 kcal/mol, distributed equally over the nine contributing dihedrals. For the C-terminal and N-terminal methyls the intrinsic term was set as zero.

The nonbonded interactions are included for atoms on different molecules and for atoms on the same molecule separated by three or more bonds. The nonbonded interactions between pairs of atoms i,j consist of a Lennard-Jones van der Waals term, with well-depth $\sigma_{i,j}$ and van der Waals radius $\epsilon_{i,j}$ and an electrostatic interaction between partial charges q_i, q_j. The dielectric constant, $\epsilon = \epsilon_0 \cdot \epsilon_r$ was set to $\epsilon = \epsilon_0$, i.e., $\epsilon_r = 1$. The electrostatic interaction energy was reduced by a factor of 0.5 for atoms separated by only three bonds. Long-range electrostatic interactions were brought to zero at a cutoff of 12 Å by applying a cubic switching function between 9 and 12 Å.[17] This truncation scheme preserves the short-range Coulombic interactions which may influence the collisional methyl dynamics, while ensuring energetic stability of the simulations. The 12 Å cutoff was chosen to be smaller than the smallest edge of the primary box to avoid interactions between an atom

and its "images" due to the application of periodic boundary conditions. Parameters for the methyl groups were obtained from a detailed examination of the gas-phase rotational barriers of linear, branched, and cyclic hydrocarbons.[22]

2. The crystal environment

The alanine dipeptide was simulated including the full crystal environment using classical molecular dynamics and periodic boundary conditions. In the periodic boundary conditions technique a primary box is constructed. Within this primary box the atoms move independently, unconstrained by any imposed symmetry. Around the primary box are constructed identical images. The atoms in the images interact with the atoms in the primary box via the nonbonded terms in Eq. (1). An atom in an image box moves identically to its corresponding atom in the primary box. To construct the crystallographic unit cell the asymmetric unit consisting of two alanine dipeptide molecules[15] was built and the corresponding orthorhombic symmetry operations of the $P_{2_12_12_1}$ space group applied. The resulting unit cell contains eight dipeptide molecules. Its dimensions are $a=13.87$ Å, $b=6.98$ Å, $c=16.29$ Å. It is preferable to work with a primary box as close to cubic as possible since this allows a maximal spherical cutoff for the electrostatic interactions. We chose our primary box to be that of two unit cells, doubling the unit cell along the b direction. The resulting primary box dimensions are $a=13.87$ Å, $b=13.96$ Å, $c=16.29$ Å. The primary box consists of 16 dipeptide molecules, i.e., 352 atoms.

3. Molecular dynamics simulations

All simulations were performed in a microcanonical ensemble using CHARMM running on the IBM 3090/600 computer at Saclay. The simulation analysis was performed with the program package *n*MOLDYN that has been recently developed.[23] The starting configuration for the simulations was obtained by minimization of the potential energy of the crystal with fixed unit cell dimensions. Simulations were performed with an integration time step of 1 fs and the bond lengths involving hydrogen atoms were constrained with the SHAKE algorithm.[24] Each simulation consisted of three phases; a 5000 step Langevin dynamics heating phase, an equilibration run of 5000 steps with occasional velocity scaling to stabilize the temperature, and the production run of 10000 steps, writing each configuration to disk. The dense spacing of the dumped configurations on the time axis is necessary for the analysis of the rigid-body motion frequency distributions where velocities have to be calculated from fitted atom postions.

C. Analysis of the simulation trajectories

1. Neutron scattering properties

A considerable part of the molecular dynamics analysis is devoted to the comparison with neutron scattering experiments since neutrons probe essentially the same time and space domain as the simulations. We briefly outline the methods used to calculate the various quantities concerned.

Dynamic structure factor. The basic measured quantity in inelastic neutron scattering experiments is the double differential cross section, $d^2\sigma/d\Omega\, dE$, which is the number of neutrons scattered into the solid angle interval $[\Omega,\Omega+d\Omega]$ and energy interval $[E,E+dE]$, normalized to $d\Omega$, dE, and the flux of the incoming neutrons,

$$\frac{d^2\sigma}{d\Omega\, dE}=N\cdot\frac{k}{k_0}S(\mathbf{q},\omega). \tag{2}$$

The quantity $S(\mathbf{q},\omega)$ is called the *dynamic structure factor*, N is the number of atoms in the sample, and k_0 and k are the moduli of the wave vectors of the incident and scattered neutrons. These are related to the corresponding neutron energies by $E_0=\hbar^2k_0^2/2m$ and $E=\hbar^2k^2/2m$, where m is the neutron mass. The energy and momentum transfer, in units of $\hbar$, are given by $\omega=(E_0-E)/\hbar$ and $\mathbf{q}=(\mathbf{k}_0-\mathbf{k})/\hbar$. The modulus of the momentum transfer is related to the energy transfer and the scattering angle Θ by

$$q=k_0\sqrt{2-\frac{\hbar\omega}{E_0}-2\sqrt{1-\frac{\hbar\omega}{E_0}}\cos(\Theta)}. \tag{3}$$

The dynamic structure factor $S(\mathbf{q},\omega)$ contains information about the structure and dynamics of the sample. It can be split into a *coherent* part arising from self- and cross-correlations of atomic motions and an *incoherent* part describing only single atom motions,

$$S_{\mathrm{coh}}(\mathbf{q},\omega)=\frac{1}{2\pi}\int_{-\infty}^{+\infty}dt\, e^{-i\omega t}\mathcal{F}_{\mathrm{coh}}(\mathbf{q},t) \tag{4}$$

$$F_{\mathrm{coh}}(\mathbf{q},t)=\frac{1}{N}\sum_{\alpha,\beta}b^*_{\alpha,\mathrm{coh}}b_{\beta,\mathrm{coh}}\langle e^{-i\mathbf{q}\cdot\mathbf{R}_\alpha(0)}e^{i\mathbf{q}\cdot\mathbf{R}_\beta(t)}\rangle, \tag{5}$$

$$S_{\mathrm{inc}}(\mathbf{q},\omega)=\frac{1}{2\pi}\int_{-\infty}^{+\infty}dt\, e^{-i\omega t}\mathcal{F}_{\mathrm{inc}}(\mathbf{q},t), \tag{6}$$

$$F_{\mathrm{inc}}(\mathbf{q},t)=\frac{1}{N}\sum_{\alpha}b^2_{\alpha,\mathrm{inc}}\langle e^{-i\mathbf{q}\cdot\mathbf{R}_\alpha(0)}e^{i\mathbf{q}\cdot\mathbf{R}_\alpha(t)}\rangle. \tag{7}$$

We see from Eqs. (4) and (6) that the coherent and incoherent dynamic structure factor are time Fourier transforms of the *coherent* and *incoherent intermediate scattering functions*, $F_{\mathrm{coh}}(\mathbf{q},t)$ and $F_{\mathrm{inc}}(\mathbf{q},t)$. α, β label individual atoms whose positions are specified by their time-dependent position vector operators $\mathbf{R}_\alpha(t)$ and $\mathbf{R}_\beta(t)$, repectively. Each atom has a *coherent scattering length* $b_{\alpha,\mathrm{coh}}$ and an *incoherent scattering length* $b_{\alpha,\mathrm{inc}}$ which defines the strength of the interaction between the nucleus of the atom and the neutron. These quantities depend only on the isotope involved.[1,4] It should be mentioned that in Eq. (2) we have tacitly assumed that multiple scattering is not present. By using the rescaled scattering lengths

$$b'_{\alpha,\mathrm{coh}}=\frac{b_{\alpha,\mathrm{coh}}}{\sqrt{\Sigma_\alpha b^2_{\alpha,\mathrm{coh}}}}, \tag{8}$$

$$b'_{\alpha,\mathrm{inc}}=\sqrt{\frac{b^2_{\alpha,\mathrm{inc}}}{\Sigma_\alpha b^2_{\alpha,\mathrm{inc}}}}, \tag{9}$$

dropping the factor $1/N$ in front of the sums, one obtains the conveniently scaled limits $F_{\mathrm{inc}}(\mathbf{q},0)=1$ and $\lim_{q\to\infty} F_{\mathrm{coh}}(\mathbf{q},0)=1$. The incoherent scattering length of hydrogen is an order of magnitude larger than the other scattering lengths in the alanine dipeptide molecule. With 12 of 22 atoms in the alanine dipeptide being hydrogen atoms we include in our calculations only the hydrogen incoherent scattering and drop the subscript "inc" in the analysis. It follows that in this case $b'_{\alpha,\mathrm{inc}}\equiv b'_{H,\mathrm{inc}}=1/\sqrt{N}$, with N being the number of hydrogen atoms in the system.

The intermediate scattering functions are quantum mechanical time-correlation functions that are replaced by classical time-correlation functions if they are calculated from MD simulations. To emphasize the classical nature of the correlation functions obtained from molecular dynamics simulations we use normal roman letters for the observables instead of the boldface letters that indicate operators. The *detailed balance condition*

$$S(\mathbf{q},\omega)=e^{\beta\hbar\omega}S(-\mathbf{q},-\omega) \tag{10}$$

does not hold in the classical limit $\hbar\to 0$. To take account of this we assume the *semiclassical correction*[4]—given here for isotropic systems, such as the polycrystalline samples under consideration,

$$\mathcal{S}(q,\omega)\approx\frac{\beta\hbar\omega}{1-e^{-\beta\hbar\omega}}S_{\mathrm{cl}}(q,\omega). \tag{11}$$

The shorthand β stands for $1/k_BT$, where k_B is Boltzmann's constant. $S_{\mathrm{cl}}(q,\omega)$ is the classical dynamic structure factor. The semiclassical correction, Eq. (11) is an approximation valid only in the linear response regime $\hbar\omega<k_BT$.

Gaussian approximation for inelastic scattering. To save CPU time $S(\mathbf{q},\omega)$ and the corresponding time-of-flight (TOF) spectra were calculated from the simulations in the *Gaussian approximation*. Using the cumulant expansion[25]

$$\langle e^{i\mathbf{q}\cdot[\mathbf{R}(t)-\mathbf{R}(0)]}\rangle=e^{-1/2\langle\{\mathbf{q}\cdot[\mathbf{R}(t)-\mathbf{R}(0)]\}^2\rangle\pm\cdots} \tag{12}$$

the intermediate incoherent scattering function can be written as

$$F(\mathbf{q},t)\approx\frac{1}{N}\sum_\alpha e^{-1/2\langle\{\mathbf{q}\cdot[\mathbf{R}_\alpha(t)-\mathbf{R}_\alpha(0)]\}^2\rangle}. \tag{13}$$

The applicability of the Gaussian approximation in the (q,ω) space of interest in the present simulations is verified in Sec. III. Since the experiments were performed on an isotropically scattering polycrystalline powder sample we averaged the exponent over all directions of $\mathbf{q}$,

$$F(q,t)\approx\frac{1}{N}\sum_\alpha e^{-q^2/6\langle[\mathbf{R}_\alpha(t)-\mathbf{R}_\alpha(0)]^2\rangle}. \tag{14}$$

The calculation of the neutron spectra in the Gaussian approximation thus involves computation of the time-dependent mean square displacements, $\langle[\mathbf{R}_\alpha(t)-\mathbf{R}_\alpha(0)]^2\rangle$. These were calculated from the molecular dynamics configurations as follows:

$$\langle[\mathbf{R}_\alpha(m)-\mathbf{R}_\alpha(0)]^2\rangle\approx\frac{1}{N_t-m}\cdot\sum_{k=0}^{N_t-m-1}[\mathbf{R}_\alpha(k+m)-\mathbf{R}_\alpha(k)]^2, \tag{15}$$

where the steps in the trajectory are denoted by $k=0,\ldots,N_t-1$. Equation (15) was evaluated using an efficient FFT-based algorithm.[26] $S(q,\omega)$ in the Gaussian approximation was obtained by numerical Fourier transformation of $F(q,t)$ as defined by Eq. (14) applying a Gauss window in the time domain[27] yielding a smoothed spectrum with a full-width half-maximum resolution of 40 cm^{-1}.

Density of States. The density of states is related to the classical dynamical structure factor by[25]

$$g(\omega)=\lim_{q\to 0}\frac{\omega^2}{q^2}S_{\mathrm{cl}}(q,\omega)=\frac{1}{N}\sum_\alpha\frac{1}{2\pi}\int_{-\infty}^{\infty}dt\,e^{-i\omega t}\langle\mathbf{v}_\alpha(0)\mathbf{v}_\alpha(t)\rangle\Big\}, \tag{16}$$

where $\langle\mathbf{v}_\alpha(0)\mathbf{v}_\alpha(t)\rangle$ is the autocorrelation function of the velocities, $\mathbf{v}_\alpha(t)$ of atom α. $g(\omega)$ can be interpreted as the kinetic energy of the hydrogen atoms in the system as a function of frequency. Equation (16) holds formally also in the quantum case.[28] $g(\omega)$ was calculated as the Fourier transform of the velocity autocorrelation function (VACF) from MD simulations. The VACF was evaluated by using a standard FFT-based algorithm for the efficient calculation of correlation functions,[29]

$$\langle\mathbf{v}_\alpha(0)\cdot\mathbf{v}_\alpha(m)\rangle\approx\frac{1}{N_t-m}\cdot\sum_{k=0}^{N_t-m-1}\mathbf{v}_\alpha(k)\cdot\mathbf{v}_\alpha(k+m). \tag{17}$$

The Fourier spectrum of the VACF was calculated applying the same windowing method as for the calculation of $S(\mathbf{q},\omega)$.

To compare to experimentally derived spectra for *finite* q values the density of states $g(q,\omega)$ was calculated from the dynamic structure factor using the first line of Eq. (16) (without performing the limit $q\to 0$) and applying the semiclassical correction formula,

$$g(q,\omega)\approx\omega\cdot\frac{1-e^{-\beta\hbar\omega}}{\beta\hbar}S(q,\omega). \tag{18}$$

The elastic incoherent structure factor. $S(\mathbf{q},\omega)$ can be divided into a part arising from purely elastic scattering with $\omega=0$ and a part with $\omega\neq 0$. Writing

$$F(\mathbf{q},t)=\mathrm{EISF}(\mathbf{q})+F'(\mathbf{q},t), \tag{19}$$

$$\mathrm{EISF}(\mathbf{q})=\lim_{t\to\infty}F(\mathbf{q},t), \tag{20}$$

where EISF stands for elastic incoherent structure factor we have

$$S(\mathbf{q},\omega)=\mathrm{EISF}(\mathbf{q})\delta(\omega)+S'(\mathbf{q},\omega). \tag{21}$$

Note here that the definition of EISF adopted here is not the same as in some analyses, in which it is a ratio of elastic

to elastic+quasielastic intensities. The EISF vanishes for all systems in which the motion of the atoms is not confined. In our case the motion of the CH_3 groups is certainly confined since the alanine dipeptide molecules form a crystal. In systems like this the EISF describes the geometry of the accessible volume and is written as follows:

$$\mathrm{EISF}(\mathbf{q})=\frac{1}{N}\sum_{\alpha}|\langle e^{i\mathbf{q}\cdot\mathbf{R}_\alpha}\rangle|^2. \tag{22}$$

As we are dealing with comparisons to scattering experiments from isotropically scattering powder samples the EISF for each atom was averaged over the directions of $\mathbf{q}$, using 100 isotropically distributed q vectors. We emphasize that the EISFs were not calculated in the Gaussian approximation—a "luxury" one can afford since for each atom only a simple time average and not a time-correlation function has to be calculated.

2. Rigid body motions

A considerable amount of the analysis is based on the study of the *rigid-body motion* of the methyl groups, i.e., the translational and rotational motion of the methyl groups as a whole, since this represents the essential information if one is less interested in their internal dynamics. The rigid-body trajectories were obtained by fitting a CH_3 reference structure into each of the 48 CH_3 groups in the primary box for each time frame and storing the Cartesian coordinates of the fitted atom positions and the parameters of the fit describing the translational and rotational degrees of freedom. As a reference structure an ideal tetrahedron was used, with the center of mass coinciding with the origin and the C atom on the z axis. The C–H bond length was chosen to be 1.1 Å which is the equilibrium distance of the harmonic C–H stretching potential, whereas the tetrahedral H–C–H angle of 109.47° differs slightly from the corresponding equilibrium value for the harmonic H–C–H bending term in the potential. For the geometrical fits of the CH_3 reference structures to the atom trajectories we used a general method to optimally superpose molecular structures that has been recently developed.[20] The method uses Hamilton's *quaternions*[30,31] for the rotational fit. Normalized quaternions can be used to parameterize rotations. The use of quaternions to find the optimal superposition of molecular structures allows the construction of a simple and efficient algorithm since the target function to be minimized can be written as a quadratic form in the quaternion parameters.

To study the methyl group motions in our given system we started from the atom trajectories $\mathbf{x}_\alpha(t=n\cdot\Delta t)\equiv\mathbf{x}_\alpha(n)$ of our molecular dynamics simulation, where $\alpha=1\cdots N$ now enumerates the atoms in a "tagged" CH_3 group, and $n=0\cdots N_t-1$ enumerates the time step. In the following we use the letter "x" for the atom positions to distinguish them from the *relative positions* with respect to the centroid position which are labeled by "r" and "X", respectively. From the atom trajectories the corresponding rigid-body trajectories

$$\mathbf{x}_\alpha^{\mathrm{rigid}}(n)=\mathbf{X}_c(n)+\mathbf{D}[\mathrm{q}(n)](\mathbf{x}_\alpha^{(0)}-\mathbf{X}_c^{(0)}) \tag{23}$$

were created where $\mathbf{x}_\alpha^{(0)}$ and $\mathbf{X}_c^{(0)}$ are the fixed positions of the atoms and the centroid in the reference structure and $\mathbf{X}_c(n)$ is the centroid of the CH_3 group at time $t=n\cdot\Delta t$ in the simulation. $\mathbf{D}(\mathrm{q})$ is a 3×3 rotation matrix expressed in quaternion parameters.[30] The centroids were chosen to coincide with the positions of the C atoms. To obtain the optimal superposition of the positions $\mathbf{x}_\alpha^{\mathrm{rigid}}(n)$ and $\mathbf{x}_\alpha(n)$ in a least-squares sense the sum of squared deviations,

$$m[q(n)]=\sum_{\alpha}w_\alpha\{\mathbf{D}[\mathrm{q}(n)]\mathbf{r}_\alpha^{(0)}-\mathbf{r}_\alpha(n)\}^2, \tag{24}$$

$$\mathbf{r}_\alpha(n)=\mathbf{x}_\alpha(n)-\mathbf{X}_c(n), \tag{25}$$

$$\mathbf{r}_\alpha^{(0)}=\mathbf{x}_\alpha^{(0)}-\mathbf{X}_c^{(0)}, \tag{26}$$

was minimized with respect to $\mathrm{q}(n)$ for each time step. The w_α are positive weights with $\Sigma_\alpha w_\alpha=1$. In our fits we used $w_{\mathrm{H}}=\frac{1}{3}$ for the hydrogens in the CH_3 groups and $w_{\mathrm{C}}=0$ for the carbon. For subsequent analysis the atom trajectories

$$\mathbf{x}_\alpha^{\mathrm{rigid}}(n),\quad n=0,\ldots,N_t-1, \tag{27}$$

and the parameter trajectories

$$\mathrm{q}(n),\quad n=0,\ldots,N_t-1, \tag{28}$$

$$\mathbf{X}_c(n),\quad n=0,\ldots,N_t-1, \tag{29}$$

were stored. The rotational motion of the CH_3 groups was studied using their angular velocities in the molecular frame which is related to the quaternions and their time derivatives by[32]

$$\begin{pmatrix}0\\ \omega_x'\\ \omega_y'\\ \omega_z'\end{pmatrix}=2\cdot\begin{pmatrix}q_0 & q_1 & q_2 & q_3\\ -q_1 & q_0 & q_3 & -q_2\\ -q_2 & -q_3 & q_0 & q_1\\ -q_3 & q_2 & -q_1 & q_0\end{pmatrix}\begin{pmatrix}\dot{q}_0\\ \dot{q}_1\\ \dot{q}_2\\ \dot{q}_3\end{pmatrix}. \tag{30}$$

The primes indicate the molecular reference system. The first line in Eq. (30) follows immediately from differentiating the normalization condition $\mathrm{q}\cdot\mathrm{q}=1$ with respect to time. To calculate the time derivative of the quaternion parameters we used a fourth-order differentiation formula for equidistantly spaced points on the abscissa.[33] To obtain sufficient precision for the derivatives a time step of 1 fs between the rigid-body configurations was used. A trajectory of the rotation angles around the molecular (x,y,z) axis can be obtained by a straightforward numerical integration of the components ω_x', ω_y', ω_z',

$$\Phi_{x,y,z}(t)=\int_0^t d\tau\,\omega_{x,y,z}'(\tau). \tag{31}$$

Simpsons rule was used with Eq. (31) to obtain the time series presented in Figs. 5(a) and 5(b).

III. RESULTS

The neutron properties reported here (elastic and inelastic scattering) give information on the motional geometry and the vibrational characteristics. For both types of scattering we report the experimental results and compare

the corresponding simulation-derived profiles before analyzing the simulations in detail. In the direct comparisons with experiment the contributions from all 182 hydrogens in the primary simulation box (including the nonmethyl hydrogens) were included. In subsequent calculations the contributions from the 32 free methyls and the 16 hindered ones are separated and further decomposed into translational and rotational components.

Experimental beam time allowed elastic scans at temperatures ranging from 20 to 325 K and inelastic measurements at two temperatures which were chosen as 150 and 300 K. Availability of data storage facilities for the rigid-body trajectories permitted simulations at three temperatures. These were chosen to be 50, 100, and 300 K, temperatures selected according to the behavior of the measured elastic scans. A combination of the data and simulation analysis is sufficient to elucidate many characteristics of the temperature-dependent dynamical behavior. Evidently the different motional characteristics and their associated scattering are somewhat interdependent. Frequent cross referencing thus allows allows one to obtain a description of the methyl dynamics that is consistent with the experimental and simulation evidence.

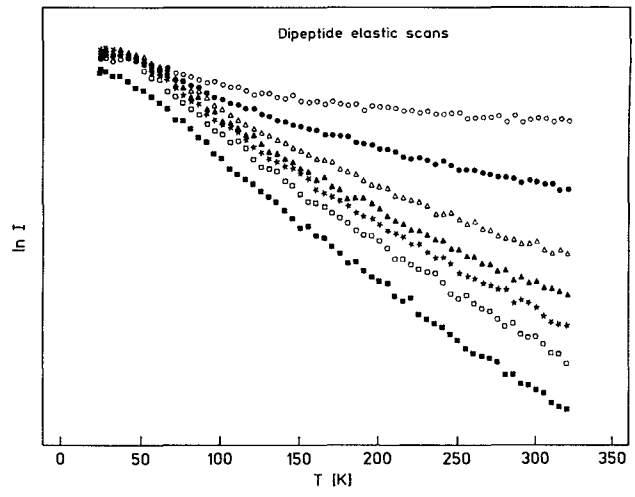

FIG. 2. Logarithm of the elastic intensity of the alanine dipeptide vs temperature at q values ranging from 0.3 Å^{-1} (upper curves) to 5.5 Å^{-1} (lower curves) obtained from experiments on IN13.

A. Elastic scattering profiles

Elastic scattering scans provide information on the geometry of the atomic motions. Any hydrogen motion will lead to a decrease in the elastic intensity at $q>0$, which is thus a maximum at $T=0$. If the hydrogen atoms undergo identical harmonic vibrations the Gaussian approximation, [Eq. (13)] is strictly valid. In this case the log of the EISF will be proportional to T at constant q and to q^2 at constant T,

$$\text{EISF}(q)=e^{-q^2\langle u^2\rangle}, \tag{32}$$

where $\langle u^2\rangle$ is the mean-square fluctuation of the (hydrogen) atoms and is proportional to T. For an isotropic, harmonic system $\langle u^2\rangle$ is $\frac{1}{6}$ times the mean-square displacement in the limit $t\to\infty$. Jump and diffusive models for conformational transitions give non-Gaussian scattering behavior.[1]

In Fig. 2 is shown log EISF vs T for the alanine dipeptide for different values of q at temperatures between 22 and 325 K. At temperatures below 50 K no significant motion is seen. The shift of the high q curve may be due to imperfect calibration of the detector concerned. A sharp decrease in the elastic intensity is seen at temperatures between $\approx$50 and $\approx$100 K followed by a decrease in the gradient at higher temperatures. The low temperature sharp decrease in elastic intensity can be interpreted as the excitation of anharmonic motions. That these motions are anharmonic is clear from the fact that the gradient does not remain constant at higher temperatures; at temperatures above $\approx$100 K the curves become close to linear (slightly concave).

The origin of the sharp low-temperature loss in elastic intensity for the dipeptide is likely to be methyl rotational motion occurring on time scale of a few hundred picoseconds or faster. Additional information on the geometry of the motions involved can be obtained by examining the q dependence of the elastic scattering. In Fig. 3(a) is shown the q dependence of the elastic scattering as derived from the IN13 experiment. Also shown is the EISF derived, using Eq. (22), from all the hydrogens in the simulations. The dashed lines represent the EISFs derived using a correction formula described below. At 300 K in both experiment and simulation there is a fast-decreasing component at low q followed by a more linear region between 6 and 25 Å^{-2}. Nonlinearity is also seen in the 100 K data, although less apparent in both the simulation and experimental curves. At 50 K both curves are almost linear, consistent with dominant vibrational motion at this temperature.

Before discussing the differences between the experimental and MD-derived elastic scattering in Fig. 3(a) we decompose the simulation-derived contributions using the methodology described in Sec. II C 2. In Fig. 3(b) is shown the contribution to the elastic scattering from the translational rigid-body motion of the free and hindered methyl groups. The hindered and free groups present almost identical translational elastic scattering, linear in q^2. This is consistent with the interpretation that collective vibrations distributed over the molecules contribute the major portion of the simulated translational dynamics. In Fig. 3(c) is presented the equivalent rotational contribution. For the free groups nonlinearity is clear at all temperatures. At 300 K a minimum is seen at 9 Å^{-2} and a subsidiary maximum at 15 Å^{-2}. The form of the curve at 300 K resembles that of the spherical Bessel function found for the elastic scattering calculated from certain dynamical models for methyl rotation.[1] Examination of the form of the 300 K rotational curve shows that it is not consistent with a three-site jump model, for which the minimum occurs at lower q values, but rather with a jump model with multiples of three sites or a diffusive model. The hindered groups have a relatively weak q dependence with some

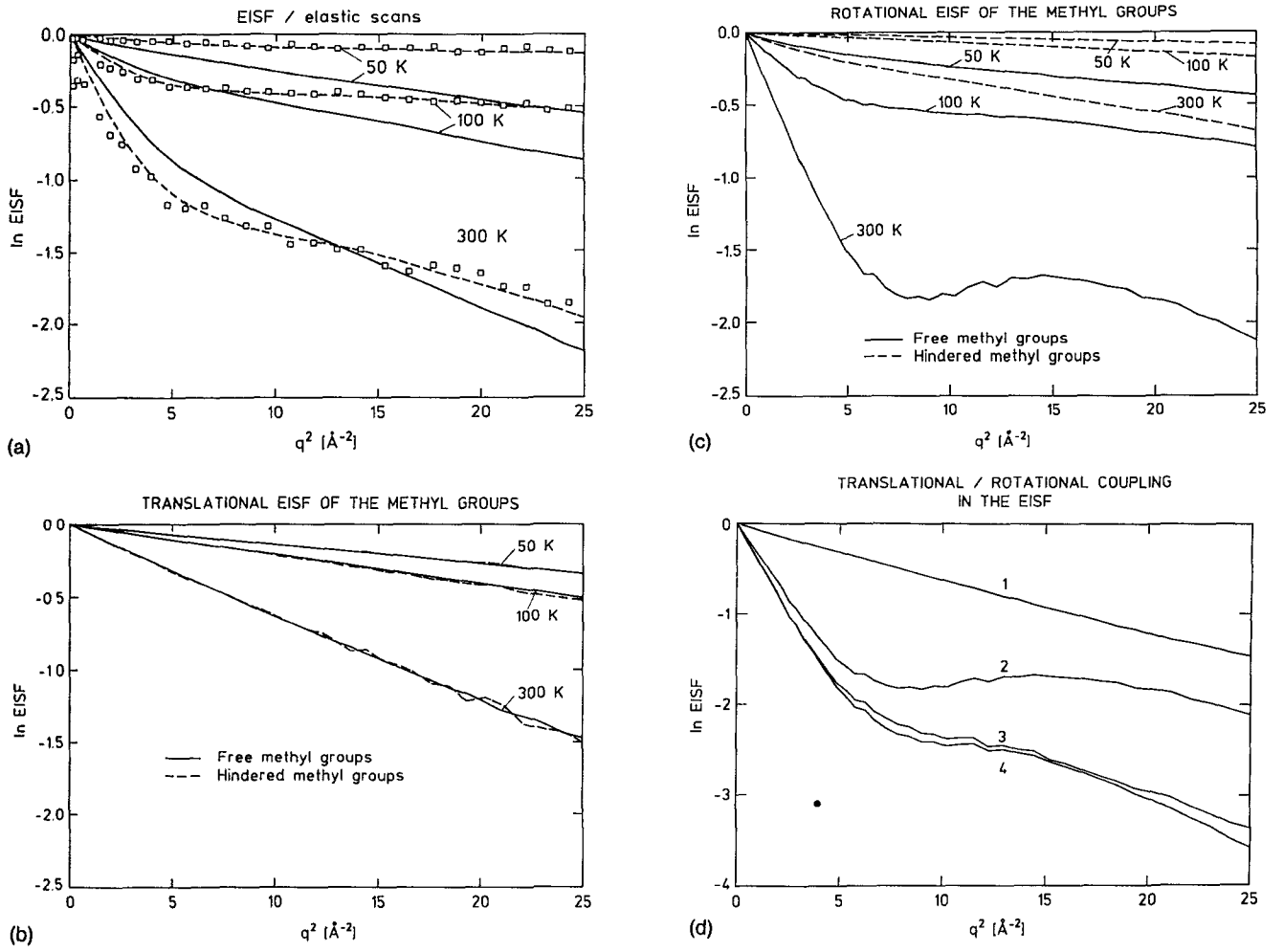

FIG. 3. Log of the elastic intensity vs q^2. (a) from the IN13 experiment (squares), the simulations (solid lines) and the using the correction formula [Eq. (35)]. The values of p, the population factor are 0 for the simulation at 50 K, 0.15 at 100 K, and 0.35 at 300 K. The corresponding values for the subtracted vibrational rms displacements, $\sqrt{\langle u_\Delta^2 \rangle}$, are 0.130 Å at 50 K, 0.133 Å at 100 K, and 0.140 Å at 300 K. (b) Translational methyl components. (c) Rotational methyl components. (d) Decomposition of the EISF at 300 K into translational and rotational components for the methyl group giving the largest error: 1—translational component, 2—rotational component, 3—full calculation, 4—product of translational and rotational components.

nonlinearity. Clearly, the hindered methyl rotational motion is not fully developed in the simulations.

It is of theoretical interest to examine whether one can justifiably separate the translational and rotational methyl contribution to the EISF, i.e., whether $\mathrm{EISF}(q) = \mathrm{EISF}_{\mathrm{trans}}(q) \cdot \mathrm{EISF}_{\mathrm{rot}}(q)$. To examine this question we calculated the rigid-body methyl group EISF as obtained by a multiplication of the rotational and translational parts and compared it with that obtained from the full rigid-body trajectory without separation. Good agreement between the two methods was obtained in all cases. The case for which the worst accord was found, a free methyl at 300 K, is shown in Fig. 3(d). The translational contribution, the rotational contribution, the product of these two contributions and the full curve calculated without assuming separability of the motions are shown. The agreement is still very good in this case indicating that the separation is valid.

The differences between the simulation-derived and experimental elastic scattering in Fig. 3(a) are as follows. At low q the experimentally derived higher temperature elastic scattering is smaller than in the simulation. Since the slope of log EISF at $q \to 0$ gives the mean-square displacement in the limit $t \to \infty$ [see Eq. (13)] this suggests that the simulation-derived mean-square displacements are smaller than the experimental values. The behavior at high q is the inverse; for all temperatures the experimentally derived elastic scattering is more intense than that derived from the simulations. The fact that, at high q, log EISF is close to linear in the simulations and experiments, together with the fact that $\log \mathrm{EISF}_{\mathrm{sim}} < \log \mathrm{EISF}_{\mathrm{exp}}$, suggests that the simulation-derived vibrational amplitudes are larger than those contributing to the normalized elastic scans.

In a comparison between the low-q experimental and simulation-derived elastic scattering one must consider the problems of instrumental resolution and of insufficient sampling of the hydrogen displacements by the simulations. The EISFs from the simulations are calculated directly as a *time average* according to Eq. (22), i.e.,

$$\mathrm{EISF}(\mathbf{q}) = \lim_{T \to \infty} \frac{1}{N} \sum_{\alpha} \frac{1}{T} \int_0^T d\tau \, | \langle e^{i\mathbf{q} \cdot \mathbf{R}_\alpha} \rangle |^2, \qquad (33)$$

making the assumption that

$$\lim_{T\to\infty}\frac{1}{T}\int_0^T d\tau\cdots\approx\frac{1}{T_{md}}\int_0^{T_{md}}d\tau\cdots, \tag{34}$$

where T_{md} is the simulation length.

In the experiment one has a different problem, that of resolving a well-sampled EISF in the *frequency domain*. T_{md} should therefore not be confused with $T_{\rm exp}=1/\Delta\nu_{\rm res}$, where $\Delta\nu_{\rm res}$ is the instrumental resolution.

With regards to the time scales, the motions can be classified into three cases. One is in which motions are too slow to be resolvable by the experiment and are poorly sampled by the simulations. The resolution of IN13 is such that only motions occuring with characteristic times faster than ≈ 1 ns can lead to a decrease in elastic intensity. A second is in which motions exist that are resolvable by the experiment and are poorly developed in the simulation. These can lead to a change in the form of the elastic intensity in Fig. 3(a) that is not seen in the simulation-derived curves. In addition, quantum mechanical tunneling effects might occur that would lead to additional motion that cannot accounted for in the simulation. A third situation is for fast motions that can be resolved by the experiment and also are well sampled in the simulations. Assuming a simple Arrhenius law for the jump rate[1] and classical motion of the methyls one arrives at the conclusion that at 100 and 50 K the discrepancy between measured and simulated elastic intensity should concern mainly the free methyls since the hindered methyls are unlikely to rotate on the timescale of the instrument either. At 300 K mainly the hindered methyls should be concerned since the free methyls are likely to be well sampled in the simulation.

The elastic scattering at high q in the simulations is increased with respect to the experiments at all temperatures. This is partly due to the fact that the experimental elastic scattering was normalized with respect to the 22 K scattering. This leads to an experimental underestimation of the vibrational mean square fluctuations at higher temperatures. A further effect may result from the fact that the same (300 K) lattice constants were used in the simulations at all temperatures. This means that at temperatures $T<300$ K the lattice dimensions are too big giving the atoms more space to move. However, the effect on the high-q EISF of a small change in the mean-square displacements is dramatic; a difference of only ≈ 0.02 Å^2 in the mean square fluctuation [5% of the 300 K vibrational mean square fluctuation in Fig. 3(b)] corresponds to a difference of 0.5 in log EISF at $q=5$ Å^{-1}. These are relatively small dynamical effects compared to the expected errors in the simulations and indicate the sensitivity of the EISF curves.

One can summarize the above considerations formally in the following "correction formula" for the EISF, designed to approximately correct for over- and underestimation of motions in the simulations,

$$\mathrm{EISF}(q)=\mathrm{EISF}_{\rm sim}(q)\cdot\frac{\mathrm{EISF}_+(q)}{\mathrm{EISF}_-(q)}. \tag{35}$$

$\mathrm{EISF}_+(q)$ is the EISF for rotational motion to be added to the simulation and $\mathrm{EISF}_-(q)$ the EISF for the vibrational motion to be subtracted from the simulation,

$$\mathrm{EISF}_+=1-p[1-A_0(q)], \tag{36}$$

$$\mathrm{EISF}_-=e^{-q^2\langle u_\Delta^2\rangle}. \tag{37}$$

In Eq. (36) p is the fraction of methyl groups not showing rotational transitions in the simulation that are seen in the experiment. $A_0(q)$ is the EISF of the additional rotational motion. For a rotational jump model this is typically a linear combination of zeroth-order spherical Bessel functions depending on the jump model assumed; which model is taken is not important since the only general behavior is of interest. In Eq. (37) $\langle u_\Delta^2\rangle$ denotes the vibrational mean-square fluctuation to be subtracted. In Fig. 3(a) the dashed lines show the corrected EISF using the the simple model described above. The parameters p and $\langle u_\Delta^2\rangle$ are given in the figure caption. p increases with T whereas $\langle u_\Delta^2\rangle$ remains constant. The latter point is consistent with the fact that the experimental elastic intensity was normalized to the scan at $T=22$ K, removing in this way the decay of the EISF due to vibrations at this temperature.

Time evolution of the mean-square displacements The time evolution of the translational and rotational mean-square displacements of the methyl hydrogens calculated from the molecular dynamics trajectories using Eq. (15) are shown in Figs. 4(a) and 4(b). In all cases there is a fast component due to vibrational motion. When this is the only type of motion present a plateau follows. In cases where additional, nonvibrational motions are present there is a slower-increasing component. Also shown, as straight lines in Fig. 4(a), are the corresponding long-time limits of the mean-square displacements as derived from the EISF. For the translational component [Fig. 4(a)] the mean square displacement increases almost exactly linearly with temperature, from 0.12 Å^2 at 100 K to 0.36 Å^2 at 300 K, again consistent with harmonic motion. However, the 50 K value, 0.08 Å^2, is somewhat higher than the harmonic model value expected from the 100 and 300 K ratio. This is consistent with an overestimation of vibrational motion in the 50 K simulation. Again the free and hindered methyl lines are very similar indicating that the translational modes are dominated by collective motions of the methyl groups. There is evidence for low-frequency vibrational structure in this correlation function, with, in particular, a maximum at 2.5 ps at 50 and 100 K lengthening to 3.0 ps at 300 K suggesting a softening of the effective potential of mean force for translational molecular motion at this temperature. The fast component lasts about 400 fs at all temperatures.

For the rotational component [Fig. 4(b)] there is a clear difference between the hindered and free methyls. The free methyls reach a plateau value of about 2.0 Å^2 at 300 K in ≈ 1 ps due to fast methyl rotational transitions. At 100 K a plateau is not reached, although a similar two-phase time evolution is seen. At 50 K the plateau value is 0.2 Å^2 and is reached more quickly, in ≈ 500 fs. A comparison of Figs. 4(a) and 4(b) indicates that 80% of

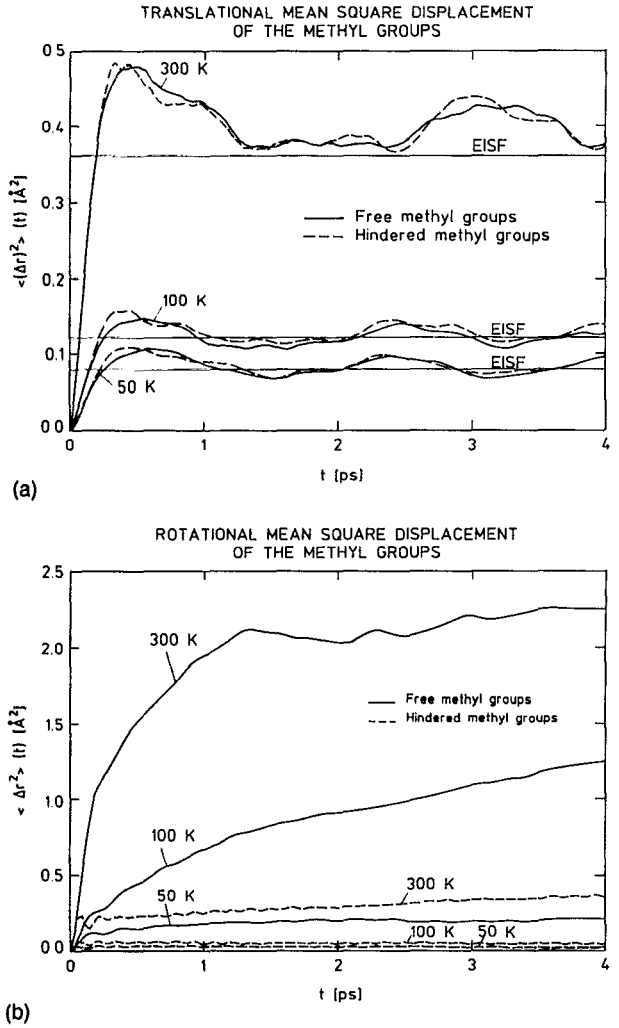

FIG. 4. Time development of the mean square displacements from the simulations. (a) translational components (b) rotational components.

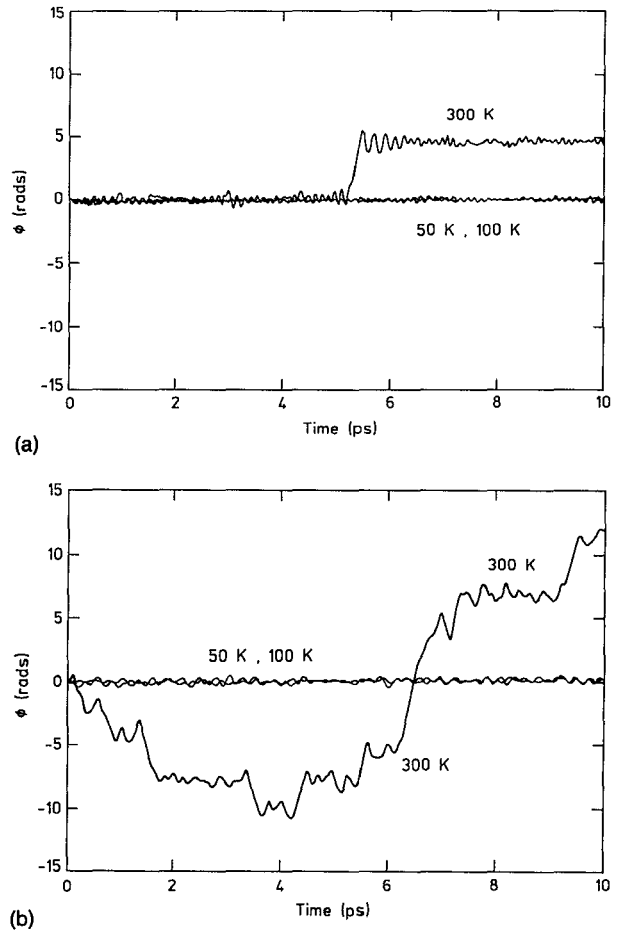

FIG. 5. Time series for the rigid-methyl dihedral angles (C_3 axis) from the simulations. (a) A hindered methyl. (b) A free methyl.

the free methyl long-time mean-square displacement is rotational at all temperatures. In contrast, for the high-barrier methyls the majority of the displacement comes from translational motion. No evidence for rotational transitions is seen. In fact one vibration dominates the establishment of the mean-square displacement, that of the torsional libration in the hindered methyl potential well. This vibration has a frequency of $\approx 220\ \mathrm{cm}^{-1}$ at 300 K. The fast component is determined by this vibration and is established within half a period, i.e., 75 fs at all temperatures. A very slowly increasing rotational slow component is seen at 150 K, suggesting some rotational diffusion of the hindered rotational potential well in the simulation.

The plateau values of the mean square displacements are much less at all temperatures in the hindered methyls, e.g., 0.8 Å^2 at 300 K compared to 2.5 Å^2 in the free case. This is largely due to the absence of methyl rotations, although an additional effect comes from the narrower potential well, i.e., smaller librational amplitudes.

B. Rotational transitions

The above results are consistent with the presence of rotational transitions of the free methyl groups on the picosecond time scale at 300 K. These motions contribute to the non-Gaussian EISF. Further experimental information on the time scale of the methyl group transitions can be obtained from an analysis of the quasielastic scattering properties of the crystals. Clear evidence for the presence of quasielastic scattering on the ps time scale was found from a preliminary analysis of the scattering profiles obtained from IN6 (not shown here). A detailed analysis of the quasielastic scattering will be published later.

Picosecond time scale rotational motion is also clearly seen in the simulations as evidenced by the EISFs and mean square displacements described in the previous section. More directly, transitions can be seen in the dihedral angle time series of the methyl groups. In Figs. 5(a) and 5(b) are shown typical time series for the methyl dihedral angles as calculated for a free and a hindered group. Only librations and no transitions for both types are seen at 50 and 100 K. At 300 K the free methyl group undergoes several rotational motions involving 2–3 rad displacements in the 10 ps time period. The time series shows diffusive characteristics. For the hindered methyl one jumplike transition is seen at 300 K, associated with a forcing of the librational oscillation.

To further examine the environment of the methyl groups rotational barriers were calculated in the crystal. This involves calculating the potential energy as a function

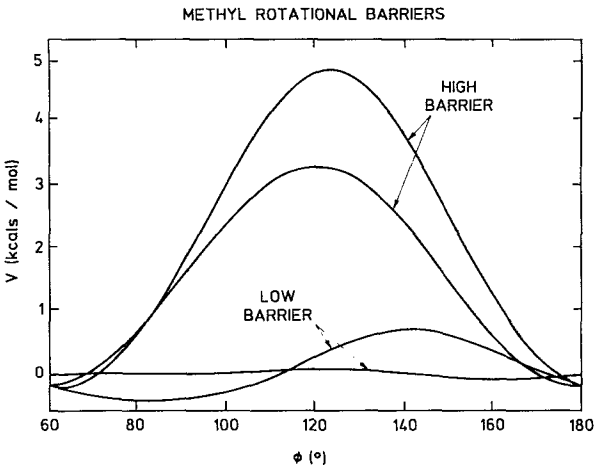

FIG. 6. Rigid-methyl rotational barrier calculations in the crystal environment. The highest and lowest barriers are presented for each of the free (low barrier) and hindered (high barrier) types of methyl group. All other barriers of a given type are in between the extremes.

of the C–C dihedral angle for each methyl group in the crystal. The four limiting case barriers are shown together in Fig. 6, i.e., the highest and lowest barriers for the free and hindered types of methyl group. Intermediate values exist in each case, due to the fact that within each type (hindered or free) there are differences in the environmental crystal-packing contribution. The results indicate that for the low barrier methyls the environmental contribution varies from 0.16 to 1.17 kcal/mol. For the hindered methyls the rigid barriers vary between 3.56 and 5.10 kcal/mol, of which 2.86 kcal/mol are contributed by the intrinsic torsional term. These values can be considered as upper limit estimates as dynamical relaxation of the surrounding atoms is not taken into account.

The results of the experimental quasielastic scattering and simulation dihedral time series and barriers are consistent with picosecond-time scale dihedral rotational transitions of the free methyl groups at 300 K.

C. Vibrational properties

Vibrational motion of the hydrogens is manifested in the inelastic scattering spectra. These are measured as TOF spectra that are nonlinear in ω. The measured spectra can be readily converted into the dynamic structure factor, $S(q,\omega)$. From $S(q,\omega)$ the density of states can be obtained. These three representations emphasize somewhat different aspects of the vibrational motion as will be described below.

1. The density of states

In Figs. 7(a) and 7(b) are shown experimental and simulation-derived densities of states at different temperatures, derived by taking the quantity $g(q,\omega)=\omega^2/q^2S(q,\omega)$ at $q=1.8$ Å^{-1} [see Eq. (16)]. The experimental 150 K $g(q,\omega)$ rises to a maximum at 142 cm^{-1}. Several other peaks are visible although the higher-frequency region >200 cm^{-1} is quite smooth. The 100 K simulation-

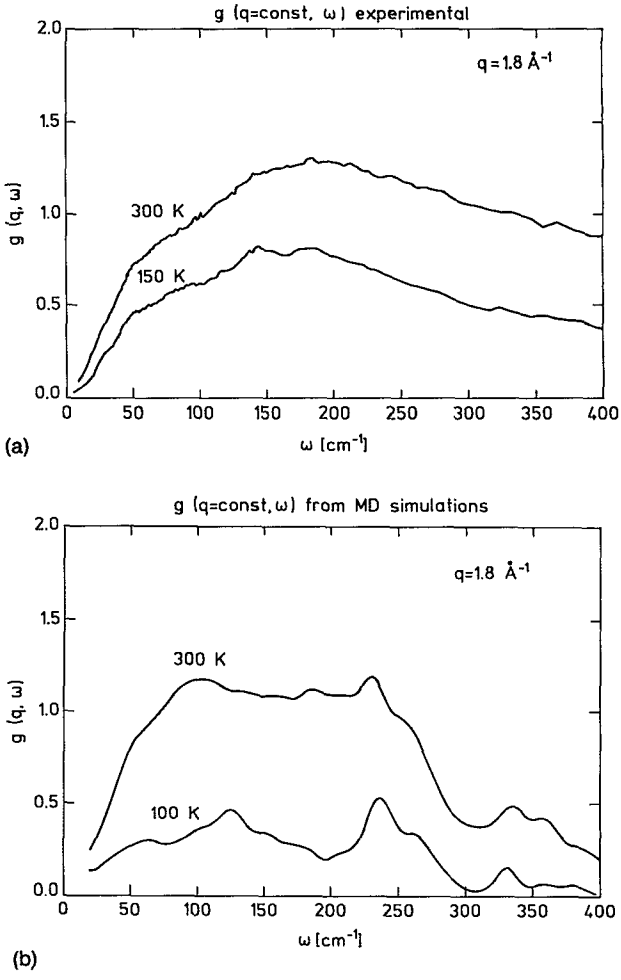

FIG. 7. $g(q,\omega)$ at $q=1.8$ Å^{-1} from (a) the IN6 experiments and (b) the simulations.

derived plot rises to a maximum at 125 cm^{-1}. Clear subsidiary peaks are present at higher frequencies; these are absent in the smoother experimental curve. At 300 K the experimental curve is smoothed, rising to a broader maximum at $\approx$200 cm^{-1}. The corresponding simulation-derived plots are also smoother than at 100 K.

The $g(q,\omega)s$ in Fig. 7 were calculated via $S(q,\omega)$ in the Gaussian approximation. We checked the validity of this approximation in this case by calculating the density of states $g(q,\omega)$ with and without invoking the Gaussian approximation at $q=5$ Å^{-1} and $T=300$ K. This is the "worst case" here since the cumulant approximation [Eq. (12)] becomes better both with decreasing q and with, due to increasing harmonicity, decreasing T. We found that $g(q,\omega)$ is very well represented by the Gaussian approximation (not shown).

The rigid-body fit allows decomposition of the simulation $g(\omega)$, i.e., the kinetic-energy weighted density of states, given by the Fourier transform of the velocity autocorrelation function as defined by Eq. (16). This function, obtained from the full and from the rigid-body trajectories at 300 K is shown in Fig. 8.

For $\omega<\approx$900 cm^{-1} the full neutron weighted $g(\omega)$ (including the hydrogen atoms that do not belong to me-

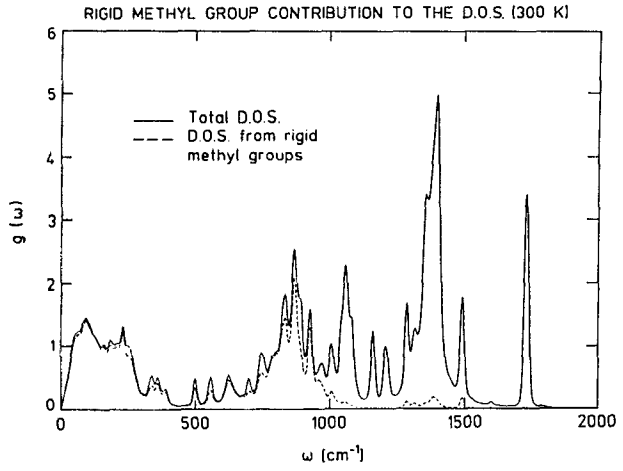

FIG. 8. $g(\omega)$ from the simulations. Full line—full trajectory. Dotted line—rigid-methyl group contribution.

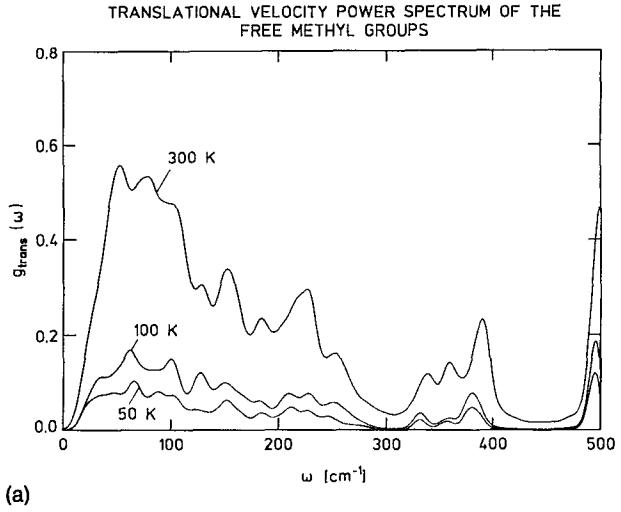

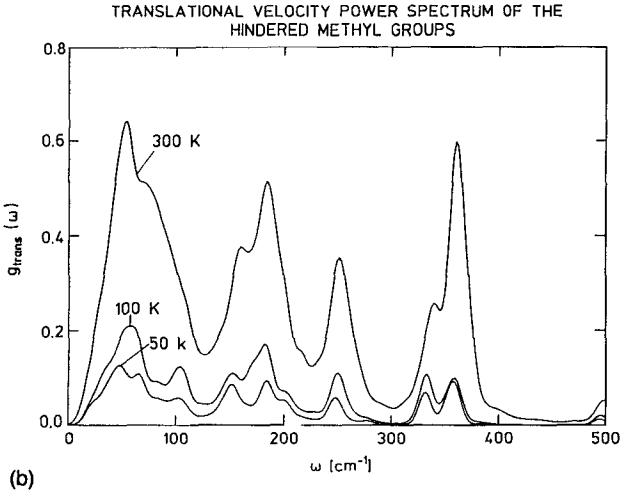

FIG. 9. Translational contribution to $g(\omega)$ for (a) free methyls, (b) hindered methyls.

thyl groups) is well represented by $g(\omega)$ resulting from rigid-body motions of the methyl groups. At higher frequencies motions involving significant displacements of the internal methyl degrees of freedom contribute.

The translational contribution to the rigid-body methyl $g(\omega)s$ is shown in Fig. 9. In all cases the zero-frequency value is zero confirming the absence of diffusive translational motion. In the power spectra of the free and hindered methyl groups there is a maximum in intensity around 40–60 cm^{-1}. We can thus assign this to the corresponding shoulder seen in the simulation-derived $g(\omega)$ and, tentatively, to the observed 50 cm^{-1} shoulder in the experimental spectra at 150 and 300 K.

The angular velocity power spectra for the free and hindered methyl rotations are shown in Figs. 10. For the free methyls the power spectra have nonzero values at zero frequency confirming the presence of rotational diffusive motion of these groups, even at 50 K. There is clear low-frequency vibrational structure at 50 K with a sharp peak at 125 cm^{-1}. This peak is due to oscillations in the effective potential well defined by the environmental nonbonded interactions. It can be assigned to the peak at 125 cm^{-1} in the full simulation plot [Fig. 7(b)] and, tentatively, to the peak at 150 cm^{-1} in the experimental spectrum. At 100 K this structure is still present but broadens considerably. At 300 K the spectrum changes qualitatively, with the 125 cm^{-1} peak disappearing and, instead torsional oscillations appearing at 15 and 100 cm^{-1}. This indicates that the free methyl groups "see" a different environment at 300 K, escaping from their various local potential minima and exploring more extended features of the potential surface.

The frequencies associated with the free methyl rotational motion are lower than those of the hindered methyl. This is consistent with the absence of the intrinsic torsional term in the potential and with the slower increase of the fast component to the mean square displacement [Fig. 4(b)]. Not surprisingly the density of states for the hindered methyl group rotation [Fig. 10(b)] is strongly influenced by the torsional libration dominated by the sinusoidal internal torsional potential. This leads to peaks at 240 and 280 cm^{-1} at 50 K. At 100 K there are only small changes in the form of these peaks. At 300 K a large change in the form and frequencies of the spectrum is again seen, with a large peak at 220 cm^{-1} appearing.

There are several differences between the experimental and theoretical $g(q,\omega)$ plots. Apart from errors in the simulation model due to periodic boundary conditions, sampling times and the potential function, further contributions should arise from multiphonon scattering and quantum mechanical effects. Nevertheless, the simulations do give some suggestions as to possible origins of some of the peaks. The 142 cm^{-1} experimental peak resembles the 125 cm^{-1} peak in the simulation, arising from environmental effects on the free methyl torsions. In a previous neutron inelastic study on N-methylacetamide,[34] the methyl groups of which are electronically similar to the free methyls in the dipeptide, the strongest scattering was also seen at $\approx$150 cm^{-1}, supporting this assignment. Transitions involving second and higher torsional excited states will not be seen in the classical dynamical simulations and could conceivably contribute to the inelastic structure in

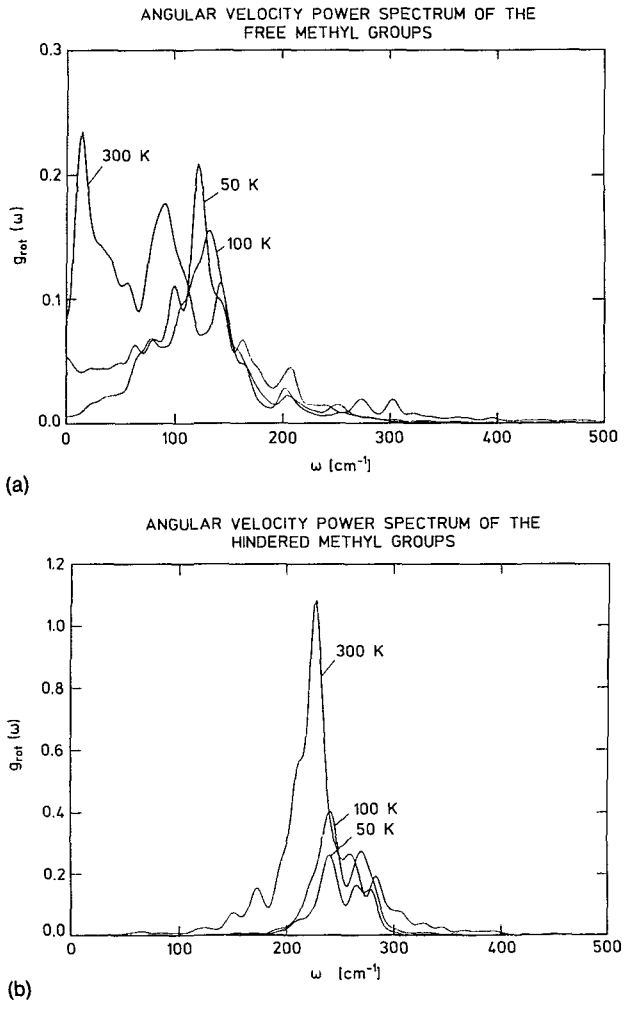

FIG. 10. Angular velocity power spectrum for motion around the methyl C_3 axis for (a) free methyls, (b) hindered methyls.

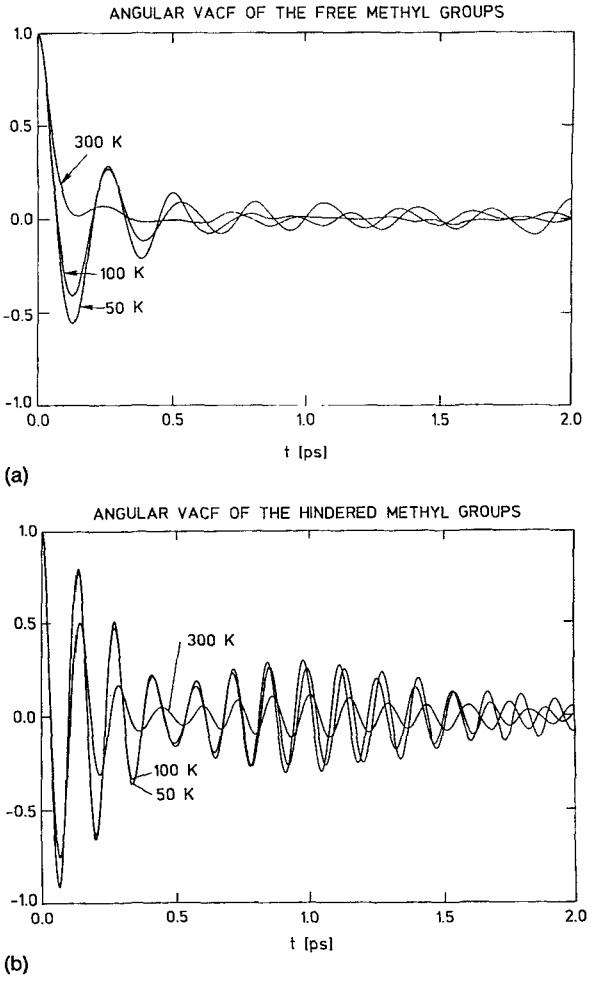

FIG. 11. Angular velocity autocorrelation function for motion around the methyl C_3 axis for (a) free methyls, (b) hindered methyls.

the experimental spectra, although there was no evidence for visible higher-level transitions in the NMA experiments.[34]

2. Velocity autocorrelation functions

Certain of the properties manifested in the simulation-derived densities of states are also seen in the velocity correlation functions. However, effects related to damping of the vibrations are more evident in the velocity autocorrelations. As an example we show in Figs. 11(a) and 11(b) the angular velocity rotational autocorrelation functions for the hindered and free methyl groups. These functions take up remarkably simple forms. At 50 and 100 K they consist of only slightly damped oscillations. Stronger damping is seen at 300 K. At all three temperatures the curves are more strongly damped in the free methyls, for which the libration is determined by nonbonded interactions with the surrounding atoms, than in the hindered groups, in which the intrinsic torsional term dominates the oscillation.

3. Time-of-flight spectra and $S(q,\omega)$

The TOF and $S(q,\omega)$ spectra give information on the amplitude-weighted frequency distributions. Experimental $S(q,\omega)$ spectra at 150 and 300 K are shown in Figs. 12(a) and 12(b). At 150 K there is structure in the inelastic region in both these profiles, superposed on the quasielastic background. A low-frequency peak is apparent in $S(q,\omega)$ at 23.2 cm^{-1} and there is a shoulder at 45 cm^{-1}. At 300 K the primary modification is a smoothing of the spectra as seen in $g(\omega)$. The low-frequency features at 23.2 and 45 cm^{-1} are still evident as shoulders in $S(q,\omega)$ indicating that they retain some vibrational character. For the lower frequency features visible on the 300 K $S(q,\omega)$ plot increased frictional damping may play a role, but an additional factor broadening this peak is swamping of the inelastic intensity by increased quasielastic scattering in this region relative to at 150 K.

In Figs. 13(a) and 13(b) the simulation-derived $S(q,\omega)$ and the corresponding frequency distributions $g(q,\omega)$ are shown at different q values. The experimental 45 cm^{-1} shoulder is present in the simulations, whereas the 23.2 cm^{-1} peak is not. The 23.2 cm^{-1} peak is possibly a lattice mode, poorly simulated using periodic boundary conditions. Even at 100 K a broadening of the quasielastic

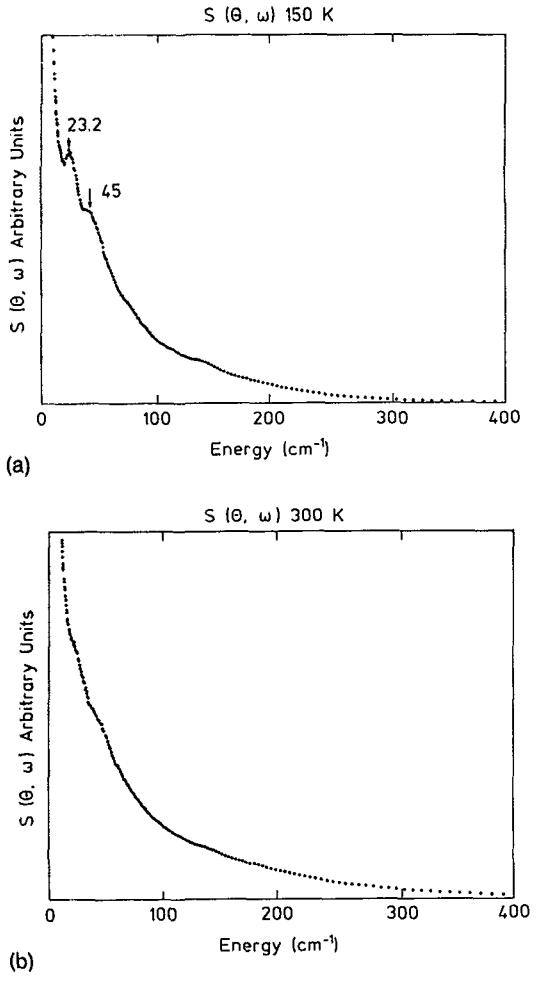

FIG. 12. Experimental $S(\theta,\omega)$ derived from IN6 experiment and averaged over several scattering angles from 19° to 111° at (a) 150 K, (b) 300 K.

line from diffusive motion on the ps time scale can be clearly seen. The features of the inelastic part of the dynamic structure factors can be better examined by looking at $g(q,\omega)$. At 100 K almost no change with increasing q can be observed, whereas at 300 K the peak at 100 cm^{-1}, already assigned to libration of the free methyl group, becomes less pronounced with increasing q. The rest of the spectrum at 300 K remains also more or less unchanged. This confirms that the librations of the free methyls are less localized than the rest of the motions and are therefore averaged out in $S(q,\omega)$ at higher q values.

Finally, the experimental and calculated TOF spectra are shown in Fig. 14. The TOF spectrum allows a convenient examination of the higher-frequency (50–250 cm^{-1}) vibrational amplitudes. The calibration of the curves in Fig. 14 was made by least-squares fitting the 300 K curves in the near inelastic region. For the 100 K curve the *same* scaling factor was applied to enable examination of the relative amplitudes of the TOF spectra. The change in amplitude and form of these spectra with temperature is reproduced reasonably well by the simulations. At low temperatures the presence of vibrational structure is clear in the experimental profile in the region (400–800 μsm^{-1}),

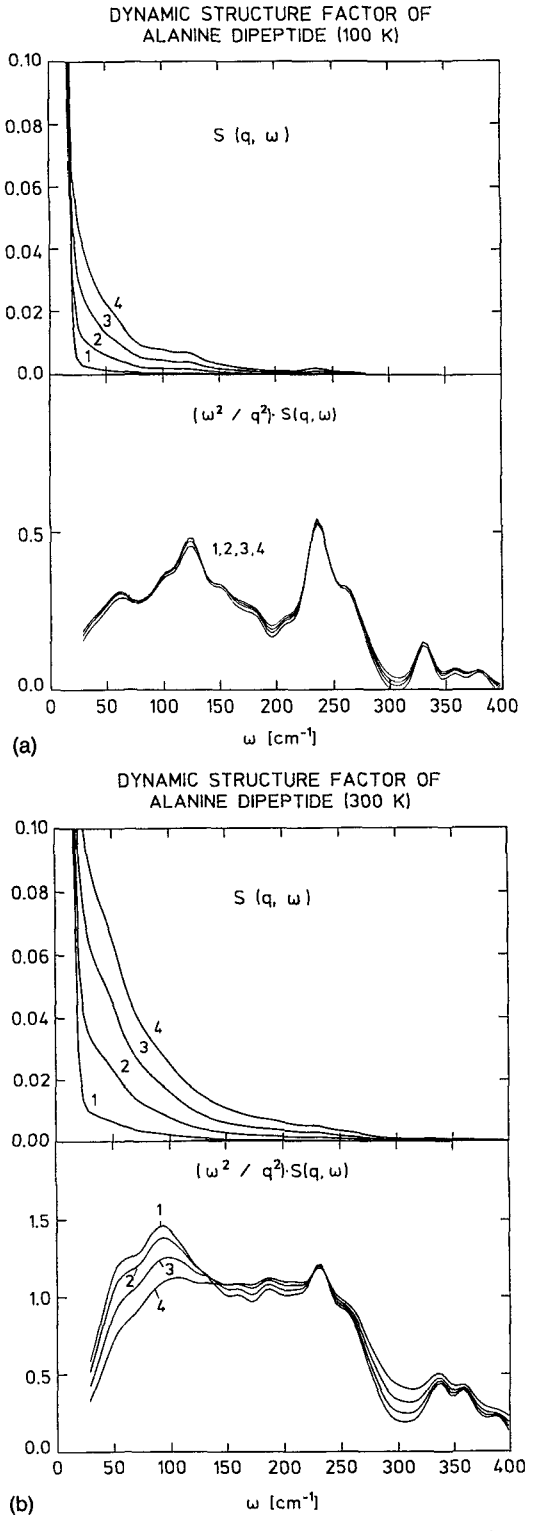

FIG. 13. $S(q,\omega)$ and $g(q,\omega)$ at different values of q ($1=0.5$ $Å^{-1}$, $2=1.0$ $Å^{-1}$, $3=1.5$ $Å^{-1}$, $4=2.0$ $Å^{-1}$) from the simulations at (a) 100 K, (b) 300 K.

culminating in a high frequency peak at 142 cm^{-1}. At 300 K the higher-frequency (100–800 μsm^{-1}) TOF spectrum presents a change in form involving a relative increase in the intensity of the high ω (low τ) scattering in both the experimental and molecular dynamics plots.

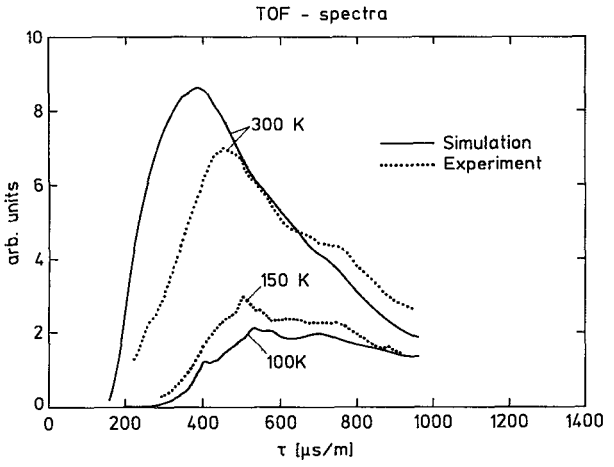

FIG. 14. Experimental and simulation-derived time-of-flight spectra averaged over several scattering angles from 19° to 111°.

IV. CONCLUDING DISCUSSION

The results reported here demonstrate the complementarity of the neutron and molecular dynamics techniques in the investigation of hydrogen atom motions in molecular crystals. This is due largely to the simple relationships between the observed neutron scattering properties and time correlation functions involving the trajectories of the hydrogen atoms. Whereas the basic characteristics of the dynamics can be defined by the experiments, the simulations can be used to provide greater detail on the nature of the motions concerned. The methyl group dynamics in the alanine dipeptide crystals are of particular interest as different methyl groups undergo very different types of motion depending on their intrinsic rotational barrier. The experimental data reported here are a superposition of these two types of motion; the simulations can be used to identify the individual contributions and to decompose the components of the time-dependent atomic position vectors to investigate the contributions of specific types of motion of interest. In the future a partial decomposition could also be achieved experimentally via selective deuteration of the side-chain or terminal groups.

Several pieces of experimental and theoretical evidence detailed in Sec. III point to the activation of C-terminal and N-terminal methyl rotations in the crystal at low temperatures. The experimental elastic scattering profiles suggest that significant anharmonic rotational motion is activated on the nanosecond time scale or faster at temperatures as low as 50–100 K. The simulations show clear evidence for activated rotational motion on the picosecond time scale, confirmed by a preliminary analysis of quasielastic neutron scattering spectra. These observations, in the light of previous quantum chemical calculations,[14] can be interpreted in terms of the existence of only a very low intrinsic methyl torsional barrier for the C-terminal and N-terminal blocking methyl groups. A consequence of this is that the rotational motion of these groups is very sensitive to the dynamical environment of the methyl groups, i.e., the influence of the close-range collisional van der Waals and, to a lesser extent, electrostatic interactions. The simulations allow these pieces of information to be incorporated into a more detailed description of the rotational dynamics.

Although several aspects of the simulation-derived neutron scattering properties are in reasonable accord with experiment quantitative agreement is not always achieved. This illustrates that even though the alanine dipeptide is a relatively simple molecule the interpretation of the experimental scattering curves is not trivial. The crystal is an inhomogeneous dynamical system. In the simulation 32 dipeptide molecules, i.e., 96 methyl groups were allowed to move independently, their positions constrained only by relatively weak nonbonded interactions. At 300 K there is clear evidence in the simulations that a highly anharmonic region of configurational space is being sampled. This leads to the question whether this region is representative of the whole configurational space.

Certain comparisons between experiment and theory do suggest possible improvements to the potential function. The exact value of the intrinsic torsional terms for the methyl groups are unknown, and additional simulations, experiments, and quantum mechanical calculations will improve this aspect. To simulate the rotational kinetics of methyl groups with significant rotational barriers in a statistically meaningful way requires either simulations much longer than are presently feasible or the use of special "activated-dynamics" techniques. The present simulations show that when the intrinsic torsional barrier is assumed as zero then the nonbonded environment results in rotational transitions on the picosecond time scale at 300 K. Whereas quantum mechanical calculations on the isolated molecule reveal N-ter and C-ter barriers of less than 0.2 kcal/mol in isolated N-methylacetamide (NMA) molecules similar calculations on hydrogen-bonded NMA suggest a slightly higher barrier, closer to 0.3–0.5 kcal/mol (Guo and Karplus, personal communication). As the alanine dipeptide is hydrogen bonded in its crystal, it is possible that a more accurate intrinsic torsional barrier may be slightly higher than that used in the present simulations. This is in accord with a shift of the experimentally derived libration peak for the free methyls at 100 K towards higher frequencies ($\approx$150 cm^{-1}) with respect to the simulation derived peak ($\approx$120 cm^{-1}).

At 100 and 50 K the free methyl atoms vibrate in effective harmonic potentials defined by the surrounding atoms. At 300 K they undergo diffusional rotational motion. The vibrations associated with this motion are damped, as evidenced by the experimental broadening of the inelastic spectra and densities of states; corresponding damping is seen in the theoretically derived spectra. There is no clear evidence for a strong peak in the experimental 300 K inelastic spectra at $\approx$220 cm^{-1} due to libration of the hindered torsional group. Although this frequency is rather high to be examined accurately with IN6 its absence in the experiments suggests that the simulation torsional barrier may be slightly wrong. A lower barrier would be consistent with certain experimentally observed peaks in the range 150–200 cm^{-1}.

The dynamics of dipeptide methyl groups may prove to be particularly useful in the study of nonbonded effects on the dynamics of picosecond time scale conformational transitions in proteins. The picosecond time scale motions occurring in a protein molecule at room temperature have both solidlike and liquidlike characteristics. The presence of low-frequency large-amplitude collective vibrations indicate solidlike behavior whereas, on the same time scale and longer there exist dynamical transitions between conformers associated with different free energy wells.[35–37] Inelastic neutron scattering experiments on myoglobin and complementary molecular dynamics simulations have produced evidence for a dynamical transition with temperature in myoglobin.[37] At temperatures below about 150 K the protein behaves as a structurally and dynamically inhomogeneous collection of vibrating molecules. At temperatures higher than this the presence of quasielastic scattering and the temperature dependence of the elastic scattering intensity indicates the presence of anharmonic motions in the protein. The dynamical origin of the associated scattering has been a subject of debate.[35,37,38] To aid in our appreciation of protein dynamics it is important to investigate systems of protein fragments, experiments and models for which can be investigated in detail and can aid in our interpretation of motions in proteins. Specifically in the case of the alanine dipeptide simulations such as these and comparisons with neutron experiments can enable the intrinsic potentials for the ϕ and ψ dihedral rotational barriers in proteins to be precisely determined. More generally, the results presented here illustrate the complexity of the dynamical phenomena present even in as simple a system as a dipeptide crystal.

ACKNOWLEDGMENTS

We acknowledge Winfried Petry for assistance with the IN13 experiment and Marc Bee and A. J. Dianoux for assistance with the IN6 experiment. We thank Victor Hruby for an initial gift of the dipeptide molecule. Financial assistance is acknowledged from the Commissariat a l'Energie Atomique, from the Bundesministerium für Forschung und Technologie (Grant No. 03-D03TUM), and from IBM France.

[1] M. Bee, *Quasielastic Neutron Scattering: Principles and Applications in Solid State Chemistry, Biology and Materials Science* (Hilger, Bristol, 1988).
[2] W. Press, *Single Particle Rotations in Molecular Crystals*, Vol. 92, Springer Tracts in Modern Physics (Springer, Berlin, 1981).
[3] D. Cavagnat, S. F. Trevino, and A. Magerl, J. Phys. Condensed Matter **1**, 10047 (1989).
[4] S. Lovesey, *Theory of Neutron Scattering from Condensed Matter*, International Series of Monographs on Physics 72 (Oxford Science, Oxford 1984).
[5] G. R. Kneller and A. Geiger, Mol. Phys. **70**, 465 (1990).
[6] J. C. Smith, S. Cusack, B. Tidor, and M. Karplus, J. Chem. Phys. **93**, 2974 (1990).
[7] J. J. Ullo, and S. Yip, J. Chem. Phys. **85**, 4056 (1986).
[8] B. M. Pettitt and M. Karplus, Chem. Phys. Lett. **121**, 194 (1985).
[9] A. Anderson, M. Carson, and J. Hermans, Ann. N.Y. Acad. Sci. **482**, 51 (1986).
[10] S. Weiss and G. E. Leroi, J. Chem. Phys. **48**, 962 (1968).
[11] R. M. Pitzer, Acc. Chem. Res. **16**, 207 (1983).
[12] D. R. Herschbach, J. Chem. Phys. **31**, 91 (1959).
[13] T. Kojima, E. Yano, K. Nakagawa, and S. Tsunekawa, J. Mol. Spectrosc. **112**, 494 (1985).
[14] H. Guo, J. Smith, M. J. Field, and M. Karplus (unpublished results). GAUSSIAN 82 calculations on methyl rotational barriers in acetaldehyde, acetamide, and N-methylacetamide were performed using complete geometry optimization for the stationary configurations at the Hartree–Fock level using polarized basis sets. Results as follows: HF/6–31*g** and MP2/6–31*g** basis sets gave 1.00 ± 0.05 kcal/mol for acetaldehyde with an eclipsed minimum (the inclusion of Moller–Plesset perturbation theory corrections for electron correlation did not significantly affect the barrier). The same basis sets gave 0.10 ± 0.05 kcal/mol for acetamide. HF/6–31*g** and HF/6–31*g*** calculations on N-methylacetamide gave 0.07 ± 0.01 kcal/mol for ψ and 0.14 kcal/mol for ϕ.
[15] Y. Harada and Y. Iitaka, Acta Cryst. B **30**, 1425 (1974).
[16] B. Maier, *Neutron Facilities at the ILL High Flux Reactor* (Institut Laue-Langevin, Grenoble, 1983).
[17] B. Brooks, R. Bruccoleri, B. Olafson, D. States, S. Swaminathan, and M. Karplus, J. Comp. Chem. **4**, 187 (1983).
[18] L. van Hove, Phys. Rev. **95**, 249 (1954).
[19] L. van Hove, Physica **24**, 404 (1958).
[20] G. R. Kneller, Mol. Simul. **7**, 113 (1991).
[21] Y. Koyama, T. Shimanouchi, M. Sato, and T. Tatsuno, Biopolymers **10**, 1059 (1971).
[22] J. C. Smith and M. Karplus, J. Am. Chem. Soc. **114**, 801 (1992).
[23] *n*MOLDYN—*A Program Package for the Analysis of Neutron Scattering Properties from Molecular Dynamics Simulations* (to be published).
[24] J. P. Rykaert, Mol. Phys. **55**, 549 (1985).
[25] J. P. Boon and S. Yip, *Molecular Hydrodynamics* (MacGraw-Hill, New York, 1980).
[26] G. R. Kneller, Report no. 2215, Kernforschungsanlage Jülich GmbH, July 1988.
[27] F. J. Harris, Proc. IEEE, **66** (1), 51 (1978).
[28] E. Clementi, G. Corongiu, M. Aida, U. Niesar, and G. R. Kneller, in MOTECC, *Modern Techniques in Computational Chemistry*, edited by E. Clementi (ESCOM, Leiden, 1990).
[29] E. O. Brigham, *The Fast Fourier Transform* (Prentice Hall, Englewood Cliffs, 1974).
[30] S. L. Altmann, *Rotations, Quaternions, and Double Groups* (Clarendon, Oxford, 1986).
[31] D. J. Evans and S. Murad, Mol. Phys. **34**, 327 (1977).
[32] G. R. Kneller and A. Geiger, Mol. Simul. **3**, 283 (1989).
[33] M. Abramowitz and I. A. Stegun, *Handbook of Mathematical Functions* (Dover, New York, 1972).
[34] F. Fillaux and J. Tomkinson, Chem. Phys. **26**, 295 (1977).
[35] J. C. Smith, Q. Rev. Biophys. **24**, 227 (1991).
[36] H. Frauenfelder, F. Parak, and R. D. Young, Ann. Rev. Biophys. Biophys. Chem. **17**, 451 (1988).
[37] W. Doster, S. Cusack, and W. Petry, Nature (London) **337**, 754 (1989).
[38] J. C. Smith, K. Kuczera, and M. Karplus, Proc. Natl. Acad. Sci. (U.S.A.) **87**, 1601 (1990).